Neuron 52, 307–320, October 19, 2006 ©2006 Elsevier Inc. DOI 10.1016/j.neuron.2006.09.012

Synapse-Specific and Developmentally Regulated Targeting of AMPA Receptors by a Family of MAGUK Scaffolding Proteins

Guillermo M. Elias,[1,5] Lars Funke,[2,4,5] Valentin Stein,[1,6] Seth G. Grant,[3] David S. Bredt,[2,7] and Roger A. Nicoll[1,2,*]
[1] Department of Cellular and Molecular Pharmacology
[2] Department of Physiology
University of California, San Francisco
San Francisco, California 94143
[3] Wellcome Trust Sanger Institute
Cambridge CB10 1SA
United Kingdom
[4] Freie Universitaet Berlin
Berlin 14195
Germany

Summary

Trafficking of AMPA receptors (AMPA-Rs) to and from synapses controls the strength of excitatory synaptic transmission. However, proteins that cluster AMPA-Rs at synapses remain poorly understood. Here we show that PSD-95-like membrane-associated guanylate kinases (PSD-MAGUKs) mediate this synaptic targeting, and we uncover a remarkable functional redundancy within this protein family. By manipulating endogenous neuronal PSD-MAGUK levels, we find that both PSD-95 and PSD-93 independently mediate AMPA-R targeting at mature synapses. We also reveal unanticipated synapse heterogeneity as loss of either PSD-95 or PSD-93 silences largely nonoverlapping populations of excitatory synapses. In adult PSD-95 and PSD-93 double knockout animals, SAP-102 is upregulated and compensates for the loss of synaptic AMPA-Rs. At immature synapses, PSD-95 and PSD-93 play little role in synaptic AMPA-R clustering; instead, SAP-102 dominates. These studies establish a PSD-MAGUK-specific regulation of AMPA-R synaptic expression that establishes and maintains glutamatergic synaptic transmission in the mammalian central nervous system.

Introduction

Glutamate acts on two types of ionotropic glutamate receptors to mediate excitatory synaptic transmission in the brain, α-amino-3-hydroxy-5-methyl-4-isoxazole propionic acid (AMPA) and N-methyl-D-aspartate (NMDA) receptors. Brief repetitive activation of excitatory synapses leads to long-term changes in synaptic strength by rapidly redistributing synaptic AMPA receptors (AMPA-Rs). Such changes may contribute to learning and memory. However, the proteins involved in AMPA-R trafficking are poorly understood. A thick electron-dense material associated with the postsynaptic membrane, referred to as the postsynaptic density (PSD), imbeds glutamate receptors. The PSD also contains scaffolding proteins, some of which contain PSD-95/Dlg/ZO-1 (PDZ) modular interaction motifs (Kim et al., 1995; Kornau et al., 1995). A particularly abundant PDZ-containing protein is PSD-95/SAP-90 (Cho et al., 1992; Kistner et al., 1993), the prototypical membrane-associated guanylate kinase (MAGUK). The PSD-95-like subfamily of MAGUKs (PSD-MAGUKs) includes PSD-93/Chapsyn-110, SAP-102, and SAP-97. PSD-MAGUKs share a common domain organization with three N-terminal PDZ domains, a Src-homology 3 (SH3) domain, and a carboxy terminal catalytically inactive guanylate kinase (GK) domain.

Determining whether PSD-MAGUKs play a role in synaptic transmission has been challenging. Whereas the PDZ domains of PSD-95 bind the C-terminal tails of NMDA receptor type-2 (NR-2) subunits (Kornau et al., 1995) and thereby cluster NMDA-Rs (Sheng, 2001), overexpression of PSD-95 selectively increases synaptic AMPA-R number (Beique and Andrade, 2003; Ehrlich and Malinow, 2004; El-Husseini et al., 2000; Nakagawa et al., 2004; Schnell et al., 2002; Stein et al., 2003). However, gene-targeted truncation of PSD-95 fails to alter synaptic transmission mediated either by NMDA receptors (NMDA-Rs) or AMPA-Rs (Migaud et al., 1998).

Several confounding factors may explain these conflicting results. PSD-MAGUK overexpression may lead to artificial protein-protein interactions. In addition, molecular redundancy among PSD-MAGUKs may lead to functional compensation, thus confounding the phenotype of knockout (KO, or −/−) mice. To determine whether PSD-MAGUKs have a role in synaptic function, we combined experimental approaches. First, we used short hairpin RNAs (shRNAs) for each PSD-MAGUK family member to acutely remove endogenous proteins. We then examined excitatory synaptic transmission in a complete PSD-95 KO mouse (PSD-95$^{-/-}$) (Yao et al., 2004), in a complete PSD-93 KO mouse (PSD-93$^{-/-}$) (McGee et al., 2001), and in a double PSD-95/PSD-93 KO mouse (PSD-95$^{-/-}$/PSD-93$^{-/-}$). Finally, we combined shRNA and overexpression experiments in PSD-MAGUK KO mice to test directly for functional redundancy and compensation. Taken together our results indicate that (1) PSD-95 and PSD-93 account for synaptic AMPA-R targeting at mature synapses, (2) PSD-95 and PSD-93 determine the synaptic content of AMPA-Rs at separate, largely nonoverlapping subsets of excitatory synapses, (3) PSD-95 and PSD-93 are jointly required for normal synaptic expression of NMDA-Rs, (4) SAP-102 functionally compensates for PSD-95 and PSD-93 in AMPA-R and NMDA-R trafficking in the PSD-95$^{-/-}$/PSD-93$^{-/-}$ mouse, and (5) the role of PSD-MAGUK proteins in synaptic AMPA-R targeting is developmentally regulated; SAP-102 is primarily responsible for clustering in neonatal synapses, whereas PSD-95 and PSD-93 primarily anchor proteins in mature synapses.

*Correspondence: nicoll@cmp.ucsf.edu
[5] These authors contributed equally to this work.
[6] Present address: Max Planck Institute of Neurobiology, Am Klopferspitz 18, 82152 Planegg-Martinsried, Germany.
[7] Present address: Department of Integrative Biology, Eli Lilly and Company, Indianapolis, Indiana 46285.

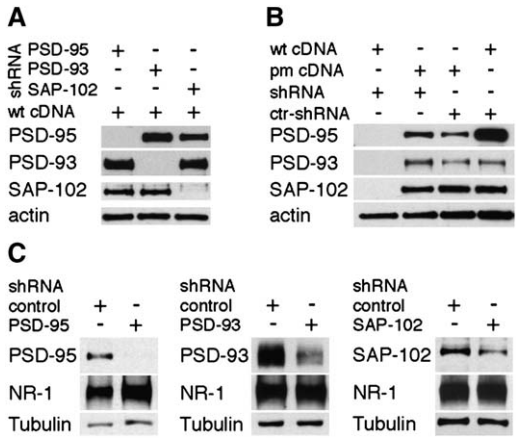

Figure 1. shRNAs Against PSD-95, PSD-93, and SAP-102 Cause Selective Knockdown in COS-7 Cells and Hippocampal Neurons

(A) COS-7 cells were cotransfected with expression vectors for PSD-95, PSD-93, or SAP-102 (wt cDNA) and an shRNA vector targeting each protein, respectively. shRNAs eliminated detectable protein for the targeted family member without affecting the other two PSD-MAGUKs.

(B) This knockdown was prevented by silent point mutations in the cDNAs of the targeted family member (pm cDNA). Control shRNA vector had no effect.

(C) Dissociated hippocampal neurons were infected with Lentivirus (~70% efficiency) containing shRNA against PSD-95, PSD-93, SAP-102, or control sequence. Protein levels of PSD-95, PSD-93, or SAP-102 are reduced by corresponding shRNAs in comparison to control virus. NR-1 and Tubulin expression levels were unchanged.

Understanding the physiological role of closely related proteins represents a recurring and challenging theme in modern biology. This study establishes novel experimental paradigms that can be broadly applied to unravel this knotty problem.

Results

shRNA Interference of PSD-MAGUKs

We first generated shRNAs against PSD-95, PSD-93, and SAP-102 and tested their efficiency and specificity by coexpression with cDNA expression vectors in COS-7 cells (Figure 1A). Knockdown of PSD-MAGUK expression was strictly specific and protein amounts were reduced below detection for each of the PSD-MAGUKs. Introducing silent point mutations in the relevant cDNAs prevents the knockdown, demonstrating target specificity (Figure 1B).

We used western blot analysis to measure the effect of shRNA on the level of PSD-MAGUK protein in primary hippocampal cultures infected with shRNA-containing Lentivirus (Figure 1C) (Lois et al., 2002). shRNA expression selectively reduced PSD-95, PSD-93, or SAP-102 protein. Lentivirus expressing a control shRNA sequence had no effect. As the infection efficiency was ~70%, these results underestimate the knockdown efficiency in infected cells. We confirmed the quantitative loss of PSD-95 protein in individual neurons by immunocytochemistry (see Figure S1 in the Supplemental Data).

shRNA of SAP-97 dramatically blocked expression of SAP-97 in COS-7 cells (not shown). However, we were unable to reduce SAP-97 protein in neuronal cultures. We tried two different shRNA constructs that were effective in COS-7 cells, and we tested multiple SAP-97 antibodies (data not shown). Thus, we are unable to address the consequences of SAP-97 deletion on synaptic transmission.

shRNA Knockdown and Gene-Targeted Deletion of PSD-95

We first examined the effect of PSD-95 shRNA. As shown in Figure 2A, surface GluR2 puncta localized at synaptic spines were greatly reduced in cultured dissociated neurons (DIV 19–21) expressing PSD-95 shRNA (42% of control). This decrease occurred without changing the density of dendritic spines (Figure 2B). Total surface GluR2 expression was effected to a similar degree ($n = 9$ cells in each condition; control = 15.9 ± 1.2 and PSD-95 shRNA = 8.2 ± 1.7 clusters per 10 μm of dendrite, $p < 0.01$). We used hippocampal slice cultures (Figures 2C–2I) to examine the effects on synaptic function. Two to three days after preparation, slices were infected with PSD-95 shRNA-carrying Lentivirus and were left for a further 5–8 days. We simultaneously recorded from an infected neuron and an uninfected neighbor and compared the synaptic responses evoked by a common input. A typical experiment is shown by the traces in Figure 2C1. As reported previously (Nakagawa et al., 2004), the AMPA-R component of the excitatory postsynaptic current (EPSC) was dramatically decreased in the infected cell, whereas there was no difference in the NMDA-R component. The results, shown in scatter plots for all neuronal pairs (Figures 2C2 and 2C3), demonstrate a 51% decrease in the size of the AMPA-R EPSC (Figure 2C2). On the other hand, there is no change in the size of the NMDA-R EPSC (Figure 2C3). These effects are target-specific, as repeating the experiment in slice cultures made from PSD-95$^{-/-}$ mice (see below) did not change either the AMPA-R (Figure 2D2) or NMDA-R EPSC (Figure 2D3). Also, using a control shRNA sequence did not effect the AMPA-R EPSC (uninfected: 49.1 ± 6.8 pA; infected: 41.9 ± 6.5 pA; $n = 16$, $p = 0.29$) (data not shown). Slow turnover of PSD-95 does not explain the remaining AMPA-R EPSC, as waiting 12–14 days after infection led to no further reduction (uninfected: 62.5 ± 5.9 pA; infected: 26.2 ± 3.5 pA; $n = 12$, $p < 0.0001$) (data not shown).

To understand the basis for the reduction in AMPA-R EPSCs, we first evaluated miniature EPSCs (mEPSCs) (Figures 2E–2G). In PSD-95 shRNA-infected neurons, there was no change in amplitude (Figure 2F) but a large decrease in event frequency (Figure 2G), suggesting that a population of synapses is silenced. To ensure that a reduction in mEPSC amplitude could be observed, we reduced evoked EPSCs to a similar extent with the AMPA-R antagonist NBQX. With NBQX, a clear reduction in mean amplitude was observed (control: −15.1 ± 1.2 pA, $n = 8$; NBQX: −8.6 ± 1.2 pA, $n = 3$; $p < 0.05$) (data not shown). To monitor silent synapses directly, we carried out minimal stimulation experiments to compare the incidence of failures in control and infected cells (Figure 2H); failure rates were consistently enhanced in the infected cells.

Where do AMPA-Rs go after they have been removed from the synapse by shRNA PSD-95? Previous experiments suggest that overexpression of PSD-95 recruits AMPA-Rs from extrasynaptic membranes to the

synapse (Schnell et al., 2002). Consistent with PSD-95 shRNA causing redistribution from synapses to extrasynaptic membranes, we found that the size of AMPA-R-mediated currents in outside-out somatic (nonsynaptic) membrane patches was enhanced (Figure 2I).

Conflicting with our shRNA data, targeted truncation of PSD-95 in mice has no effect on synaptic transmission (Migaud et al., 1998). Might the difference be due to the remaining expression of the N-terminal fragment of PSD-95 in this mouse (Migaud et al., 1998), which is necessary and sufficient for the overexpression enhancement (Schnell et al., 2002)? To address this, we examined synaptic transmission in acute hippocampal slices from postnatal day 30 to 40 (P30–40) mice that completely lack PSD-95 protein (Yao et al., 2004) (Figures 2J and 2K). First, we used extracellular field potential recording to compare the strength of synaptic transmission between control and PSD-95$^{-/-}$ mice. The size of the presynaptic fiber volley (input) was compared to the size of the field excitatory postsynaptic potential (fEPSP) response (output). Over a range of stimulus strengths, no differences were observed between PSD-95$^{-/-}$ and control mice (Figure 2J). Next, we compared the size of the AMPA-R EPSC to that of the NMDA-R EPSC. In contrast to our shRNA experiments, we found no difference in the AMPA/NMDA EPSC ratio (Figure 2K), indicating that synaptic transmission is normal in the PSD-95$^{-/-}$ mouse.

Effects of shRNA Knockdown and Gene-Targeted Deletion of PSD-93

Do other PSD-MAGUKs play a role in glutamate receptor synaptic clustering? We examined the role of PSD-93, which also localizes to dendritic spines in CA1 hippocampal pyramidal neurons (Figure 3A). PSD-93 overexpression strongly enhances AMPA-R EPSCs (Figures 3B1 and 3B2). This enhancement was receptor-selective, as there was no change in NMDA-R EPSCs (Figures 3B1 and 3B3). In addition, shRNA knockdown of PSD-93 caused a 48% selective reduction in the size of the AMPA-R EPSC (Figures 3C1 and 3C2), with no change in NMDA-R EPSCs (Figures 3C1 and 3C3). This effect on AMPA-R transmission is target-specific; repeating the same experiment in the PSD-93$^{-/-}$mouse had no effect (Figures 3D1–3D3). We examined the mechanism for this reduction by recording mEPSCs. Similar to the results with PSD-95 shRNA, depletion of PSD-93 had no effect on the amplitude of mEPSCs (Figures 3E and 3F), but did cause a clear reduction of the frequency of mEPSCs (Figure 3G), suggesting that AMPA-Rs are lost from a subset of synapses.

We also analyzed synaptic transmission in the hippocampus of the PSD-93$^{-/-}$ mouse (McGee et al., 2001). We first used field potential recordings to evaluate the strength of synaptic transmission. No difference in synaptic strength was found (Figure 3H). Next we examined the relative contribution of AMPA and NMDA receptors to the synaptic response (Figure 3I); again, no difference could be detected.

The Effects of Gene-Targeted Double Knockout of PSD-95 and PSD-93 on Synaptic Transmission

As shRNA to either PSD-95 or PSD-93 diminish synaptic targeting of AMPA-Rs, perhaps functional redundancy masks synaptic deficits in the single KO mice. To address this, we generated PSD-95/PSD-93 double KOs. Unlike the single KOs, which were grossly indistinguishable from their littermates, PSD-95$^{-/-}$/PSD-93$^{-/-}$ mice were clearly impaired. By 3 to 5 weeks of age, these animals were noticeably smaller than control littermates (Figure 4A) and typically died unless special care was provided from weaning onward. The animals had impaired gait and were markedly hypokinetic (see Movie S1 in the Supplemental Data). In these animals, field input/output curves revealed a 55% reduction in synaptic transmission (Figure 4B). Furthermore, the AMPA/NMDA EPSC ratio was reduced ~50% (Figure 4C). These decreases occurred without any change in paired pulse facilitation (PPF) (Figure 4G), indicating that the probability of transmitter release was unaltered. Interestingly, as with shRNA knockdown of PSD-95 or PSD-93, the amplitude of mEPSCs was unchanged (Figures 4D and 4E), but there was a dramatic reduction in the frequency (Figures 4D and 4F).

Western blotting of PSD-95$^{-/-}$/PSD-93$^{-/-}$ hippocampal homogenates and littermate controls showed no difference in the total amounts of GluR1, GluR2, and NR-1 (Figures 4H and 4I). However, in accord with the electrophysiological data, the PSD-enriched fraction (TritonX 100 insoluble) showed a significant loss of GluR1 and GluR2 (Figures 4J and 4K), while NR-1 remained unchanged.

Role of SAP-102 in Synaptic Transmission

What might account for the remaining transmission in the PSD-95$^{-/-}$/PSD-93$^{-/-}$ mice? As this remaining transmission greatly exceeds the subtractive effects of the combined individual shRNA-mediated knockdowns, some type of compensation has presumably occurred. Might other PSD-MAGUKs contribute to clustering synaptic AMPA-Rs? We first carried out western blotting on hippocampal homogenates from PSD-95$^{-/-}$/PSD-93$^{-/-}$ mice and found no change in the total level of SAP-97, whereas SAP-102 expression was increased by about 20% (Figure 5A). Similar results were obtained for the PSD-enriched fraction (Figure 5B). These results suggest that SAP-102 may cluster the AMPA-Rs that mediate the remaining synaptic transmission.

Previous studies showed that overexpression of SAP-102 selectively enhances AMPA-R EPSCs (Schnell et al., 2002). However, in the present study we found that knockdown of endogenous SAP-102 with shRNA had no effect on basal synaptic transmission (Figures 5C1–5C3), indicating that SAP-102 is not required for synaptic AMPA or NMDA receptor expression at mature synapses. In striking contrast SAP-102 shRNA expression in slice cultures from PSD-95$^{-/-}$/PSD-93$^{-/-}$ mice caused a 52% reduction in the remaining transmission (equivalent to 82.5% from wild-type) (Figures 5D1 and 5D2). There was also a small reduction in the NMDA-R component (Figure 5D3). No change in PPF was detected (Figure 5E), indicating a postsynaptic change. Concomitant with the reduction in evoked synaptic transmission, AMPA-R-mediated mEPSC amplitude was decreased and frequency was further decreased (Figures 6A–6C), suggesting removal of AMPA-Rs from all of the remaining synapses.

The depression of the NMDA-R EPSC is the first functional evidence that PSD-MAGUKs may, in fact, play

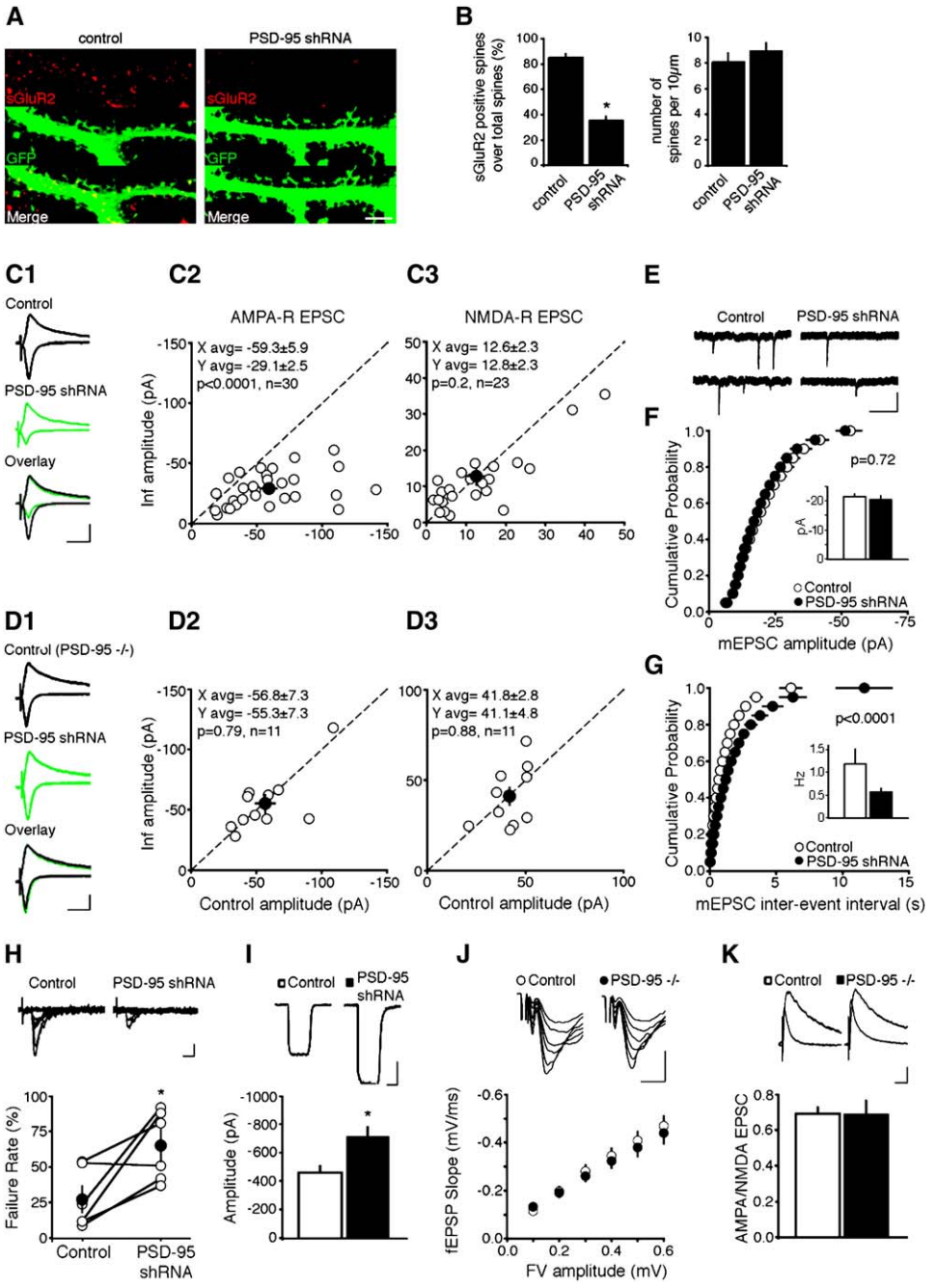

Figure 2. PSD-95 Is Necessary for AMPA-R Clustering in a Subset of Synapses

(A) Dissociated rat hippocampal neurons infected with GFP (to visualize spine structure) and shRNA against PSD-95 showed a significant reduction in surface GluR2 (sGluR2) clusters compared with neurons infected with GFP only. Scale bar, 5 μm.

(B) The number of sGluR2-positive spines in PSD-95 shRNA infected neurons was reduced ~50% (right panel) with no effect on total spine number (n = 9 cells for each condition, *p < 0.05). Error bars = SEM.

(C1–D3) For scatter plots, open circles represent amplitudes for single pairs and filled circles represent the mean ± SEM. (C1) Traces of evoked EPSCs recorded simultaneously from an uninfected wild-type neuron (top) and a neighbor infected with PSD-95 shRNA Lentivirus (middle). Distributions of EPSC amplitudes show a significant reduction in the AMPA-R EPSC (C2) but no change in the NMDA-R EPSC (C3). (D1) Traces of simultaneously recorded evoked EPSCs in pyramidal neurons from PSD-95$^{-/-}$ mice showing that PSD-95 shRNA expression has no effect on AMPA-R (D2) or NMDA-R (D3) EPSCs. (C1) and (D1) scale bars, 50 pA, 50 ms.

(E–G) mEPSC sample traces ([E], scale bar: 20 pA, 250 ms) showing that shRNA-mediated knockdown of PSD-95 does not affect the mEPSC amplitude ([F], n = 9 pairs) but strongly reduces mEPSC frequency ([G], n = 15 pairs). Error bars = SEM.

(H) (Top) Superimposed traces showing responses to minimal stimulation from a control uninfected cell (left) and a PSD-95 shRNA-expressing cell (right). Scale bar, 25 pA, 10 ms. (Bottom) Pairwise comparison reveals a significantly larger incidence of failures in PSD-95 shRNA infected cells (uninfected: 27.3% ± 8.5%; infected: 65.2% ± 10%; n = 6 pairs, *p < 0.05).

(I) (Top) Traces of AMPA-evoked currents from outside-out somatic patches in uninfected control and PSD-95 shRNA-expressing cells. Scale bar, 250 pA, 1 s. (Bottom) PSD-95 knockdown significantly increases extrasynaptic AMPA-R responses (uninfected: 461.6 ± 46.1, n = 11; infected: 717.2 ± 62.7, n = 5; *p < 0.05). Error bars = SEM.

a role in synaptic targeting of NMDA-Rs. Given this unexpected finding, we wished to ensure that this effect was not nonspecific. Therefore, we compared the effect of SAP-102 shRNA on the AMPA-R EPSC and the inhibitory postsynaptic current (IPSC) in slices from PSD-95$^{-/-}$/PSD-93$^{-/-}$ mice. In the presence of the NMDA-R blocker APV, we measured the size of the AMPA-R EPSC at −60 mV, the reversal potential for the IPSC, and then measured the size of the IPSC at 0 mV, the reversal potential for the EPSC. The depression of the AMPA-R EPSC by SAP-102 shRNA was not accompanied by any change in the IPSC (Figures 6D1–6D3). These experiments, as well as the fact that SAP-102 shRNA in mature wild-type mouse slices had no effect, establish the specificity of the effects on both the AMPA-R and NMDA-R EPSCs.

Our results show that shRNA-mediated knockdown of either PSD-95 or PSD-93 results in an ~50% reduction in the AMPA-R EPSC. In PSD-95$^{-/-}$/PSD-93$^{-/-}$ mice, AMPA-R-mediated transmission is reduced by 55%. In these mice, SAP-102 is upregulated and is responsible for targeting much of the remaining AMPA-Rs. Taken together, these results suggest that PSD-95 and PSD-93 determine the synaptic expression of most, if not all, AMPA-Rs. Accordingly, simultaneous knockdown of PSD-95 and PSD-93 should reduce transmission by significantly more than 50%. To test this, we infected wild-type slices with Lentiviral particles expressing PSD-95 shRNA and dsRed in parallel with particles expressing PSD-93 shRNA and EGFP. A substantial number of cells expressed both constructs (Figure 7A). In doubly infected cells AMPA-R-mediated synaptic transmission was reduced ~75% (Figures 7B1 and 7B2). Note that there is also a reduction in the NMDA-R component accompanying the dramatic loss of AMPA-Rs (Figure 7B3). No significant change in PPF was detected (control: 1.6 ± 0.1; infected: 2.0 ± 0.2; n = 15, p = 0.07, data not shown), suggesting an entirely postsynaptic effect. These results with acute double shRNA are more dramatic than in the PSD-95$^{-/-}$/PSD-93$^{-/-}$ mouse, but resemble results obtained with SAP-102 shRNA in the PSD-95$^{-/-}$/PSD-93$^{-/-}$ background. To ensure that the effects caused by the double shRNA are specific, we repeated these experiments in slices from PSD-95$^{-/-}$/PSD-93$^{-/-}$ mice (Figures 7C1–7C3). No effect was observed, indicating the specificity of the results in the wild-type slices. Taken together, these results strongly suggest that (1) when PSD-MAGUKs are deleted in the germ line, other PSD-MAGUKs can compensate, and (2) PSD-MAGUKs are essential for targeting nearly all AMPA-Rs to the synapse.

PSD-MAGUK-Specific Developmental Regulation of Synaptic AMPA-R Targeting

During development SAP-102 is expressed strongly by P10, whereas robust expression of PSD-95 and PSD-93 occurs 3 weeks later (Sans et al., 2000). The impairment in PSD-95$^{-/-}$/PSD-93$^{-/-}$ mice (Figure 4) matched this developmental expression profile. Thus, 1 week old PSD-95$^{-/-}$/PSD-93$^{-/-}$ mice were indistinguishable from their littermates (Figure 8A). Moreover, 1 week old PSD-95$^{-/-}$/PSD-93$^{-/-}$ mice showed no difference in the AMPA/NMDA ratio (Figure 8B), mEPSC amplitude (Figures 8C and 8D), or mEPSC frequency (Figure 8E). Furthermore, shRNA knockdown of PSD-95 did not affect synaptic transmission in immature synapses (Figures 8F1–8F3). Whereas SAP-102 shRNA had no effect on mature synapses (Figures 5C1–5C3), SAP-102 shRNA caused an ~50% reduction specifically in AMPA-R-mediated synaptic transmission in immature synapses (Figures 8G1–8G3). This establishes SAP-102 as the dominant PSD-MAGUK for AMPA-R trafficking during early postnatal development.

Discussion

These results provide important new mechanistic insights into synaptic AMPA-R targeting. They also compare the utility of two widely used loss-of-function approaches—gene targeting and RNA interference (RNAi)-mediated knockdown. Acute knockdown with shRNA shows that PSD-95 and PSD-93 normally mediate AMPA-R targeting to mature synapses. Interestingly, these knockdowns silence a population of synapses and have no effect on the remaining synapses, which indicates unexpected synaptic heterogeneity. Mice genetically lacking either PSD-95 or PSD-93 show little defect in synaptic transmission. This reflects redundancy, as PSD-95$^{-/-}$/PSD-93$^{-/-}$ mice show a clear defect. SAP-102 has no role at mature synapses, but is upregulated in the PSD-95$^{-/-}$/PSD-93$^{-/-}$ mouse to mediate residual transmission. At immature synapses, PSD-95 and PSD-93 play a minor role, whereas SAP-102 is primarily responsible for synaptic targeting of AMPA-Rs. Our results show a remarkable orchestration by PSD-MAGUKs in synaptic trafficking of AMPA-Rs.

Overexpression of PSD-MAGUKs

In a previous study, we reported that overexpression of PSD-95 and SAP-102 enhanced AMPA-R EPSCs, while overexpression of SAP-97 had no effect (Schnell et al., 2002). Similar results with PSD-95 have been reported (Beique and Andrade, 2003; Ehrlich and Malinow, 2004; Nakagawa et al., 2004). More recent studies have reported that SAP-97 overexpression causes a modest enhancement of EPSCs both in slice culture (Nakagawa et al., 2004) and in dissociated neurons (Rumbaugh et al., 2003). What might account for the different results? In one study it was found that only one splice variant of SAP-97 caused the enhancement in EPSCs (Rumbaugh et al., 2003). However, we used this variant in our past and present experiments, which involved expressing the untagged wild-type construct (data not shown). In a final set of experiments we found that PSD-93 selectively enhanced AMPA-R EPSCs. In summary, based on our experiments, overexpression

(J) (Top) Traces of AMPA-R-mediated field responses recorded from acute hippocampal slices from PSD-95$^{-/-}$ and control mice. Scale bar, 0.5 mV, 5 ms. (Bottom) Input-output curve showing that for each input (FV, fiber volley), the output (fEPSP) is unchanged in the PSD-95$^{-/-}$ relative to controls. Each point represents the mean ± SEM for each fiber volley (controls, n = 56; PSD-95$^{-/-}$, n = 26; p > 0.05 for all fiber volleys).
(K) (Top) NMDA-R and AMPA-R EPSCs from PSD-95$^{-/-}$ and controls. Scale bar, 25 pA, 50 ms. (Bottom) Bar graphs showing no difference in the AMPA/NMDA EPSC ratio (controls: 0.69 ± 0.04, n = 40; PSD-95$^{-/-}$: 0.69 ± 0.08, n = 20; p = 0.94). Error bars = SEM.

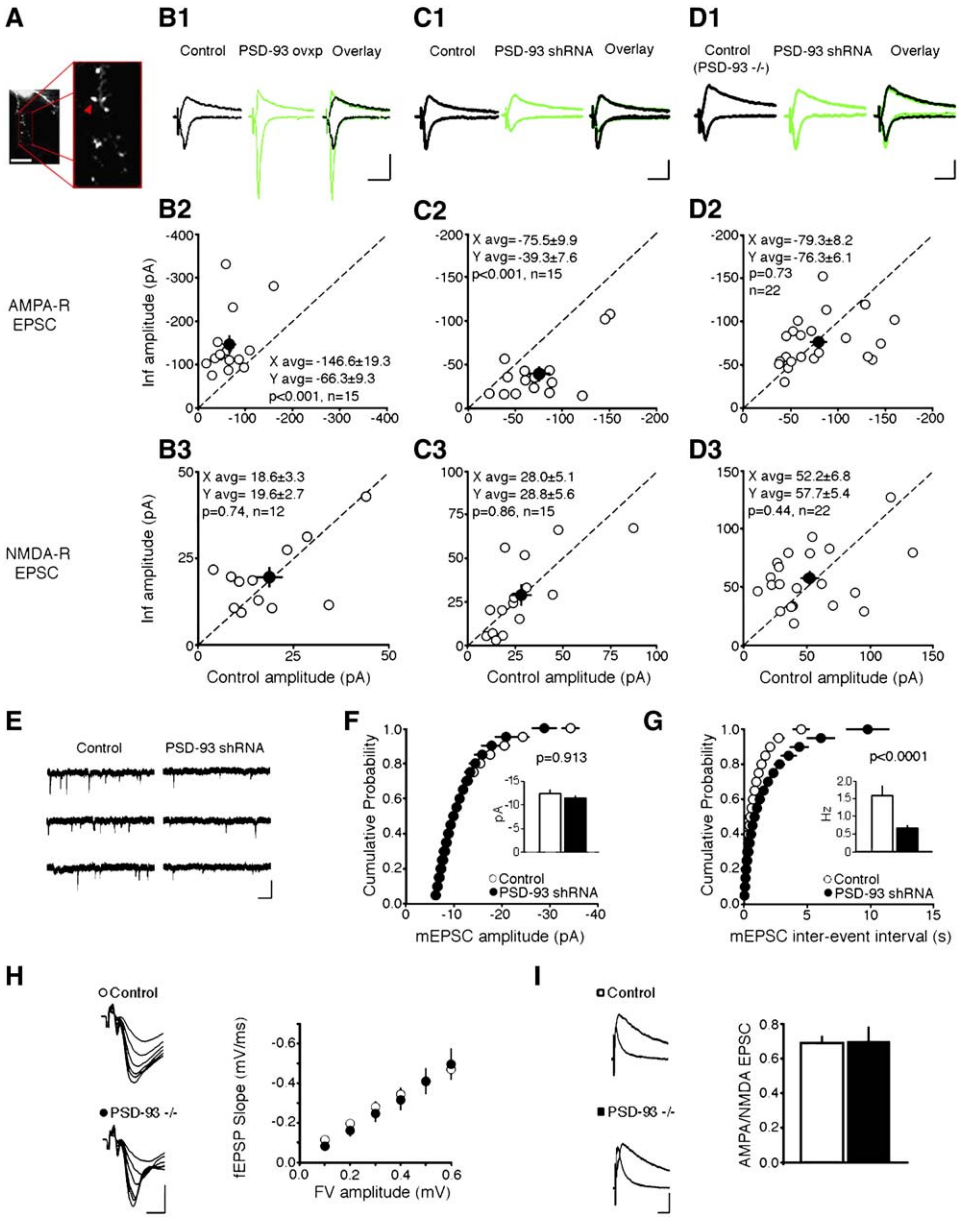

Figure 3. PSD-93 Is Necessary for Clustering of AMPA-R in a Subset of Synapses

(A) Fluorescent image showing appropriate targeting of GFP-PSD-93 fusion protein to dendritic spines (inset, red arrow). Scale bar, 50 μm.

(B1–D3) Open and filled circles represent amplitudes for single pairs and mean ± SEM, respectively. (B1) Traces of evoked EPSCs recorded simultaneously from an uninfected neuron (left) and a neighbor overexpressing PSD-93 (middle). Distributions show enhancement in the AMPA-R EPSC (B2) but no change in the NMDA-R EPSC (B3). (C1) Traces of evoked EPSCs from an uninfected neuron (left) and a neighbor expressing PSD-93 shRNA (middle). Distributions show a reduction in the AMPA-R EPSC (C2) but no change in the NMDA-R EPSC (C3). (D1) Traces showing that PSD-93 shRNA expression in neurons from PSD-93$^{-/-}$ mice has no effect on AMPA-R (D2) or NMDA-R (D3) EPSCs. Scale bars for (B1), (C1), (D1), 50 pA, 50 ms.

(E–G) mEPSC traces ([E], scale bar, 25 pA, 250 ms) showing that shRNA-mediated knockdown of PSD-93 does not affect mEPSC amplitude ([F], n = 15) but does reduce frequency ([G], n = 15). Error bars = SEM.

(H) Sample traces of field responses recorded from PSD-93$^{-/-}$ and controls. Scale bar, 0.5 mV, 5 ms. Input-output curve showing that for each fiber volley the fEPSP is unchanged in PSD-93$^{-/-}$ (controls: n = 56; PSD-93$^{-/-}$: n = 16). $p > 0.05$ for every fiber volley. Error bars = SEM.

(I) Sample NMDA-R and AMPA-R EPSCs from representative cells. Scale bar, 25 pA, 50 ms. (Right) Bar graphs showing no difference in the AMPA/NMDA EPSC ratio (control: 0.69 ± 0.04, n = 40; PSD-93$^{-/-}$: 0.7 ± 0.08, n = 11; p = 0.92). Error bars = SEM.

of PSD-95, PSD-93, and SAP-102, but not SAP-97, robustly and selectively enhances AMPA-R EPSCs. However, it has remained unclear whether these findings, based on overexpression, have any physiological relevance.

shRNA Knockdown of PSD-MAGUKs

Our generation of shRNAs that selectively and dramatically knock down expression of PSD-95, PSD-93, and SAP-102 allowed us to address this issue. Knockdown of either PSD-95 or PSD-93 resulted in a selective 50%

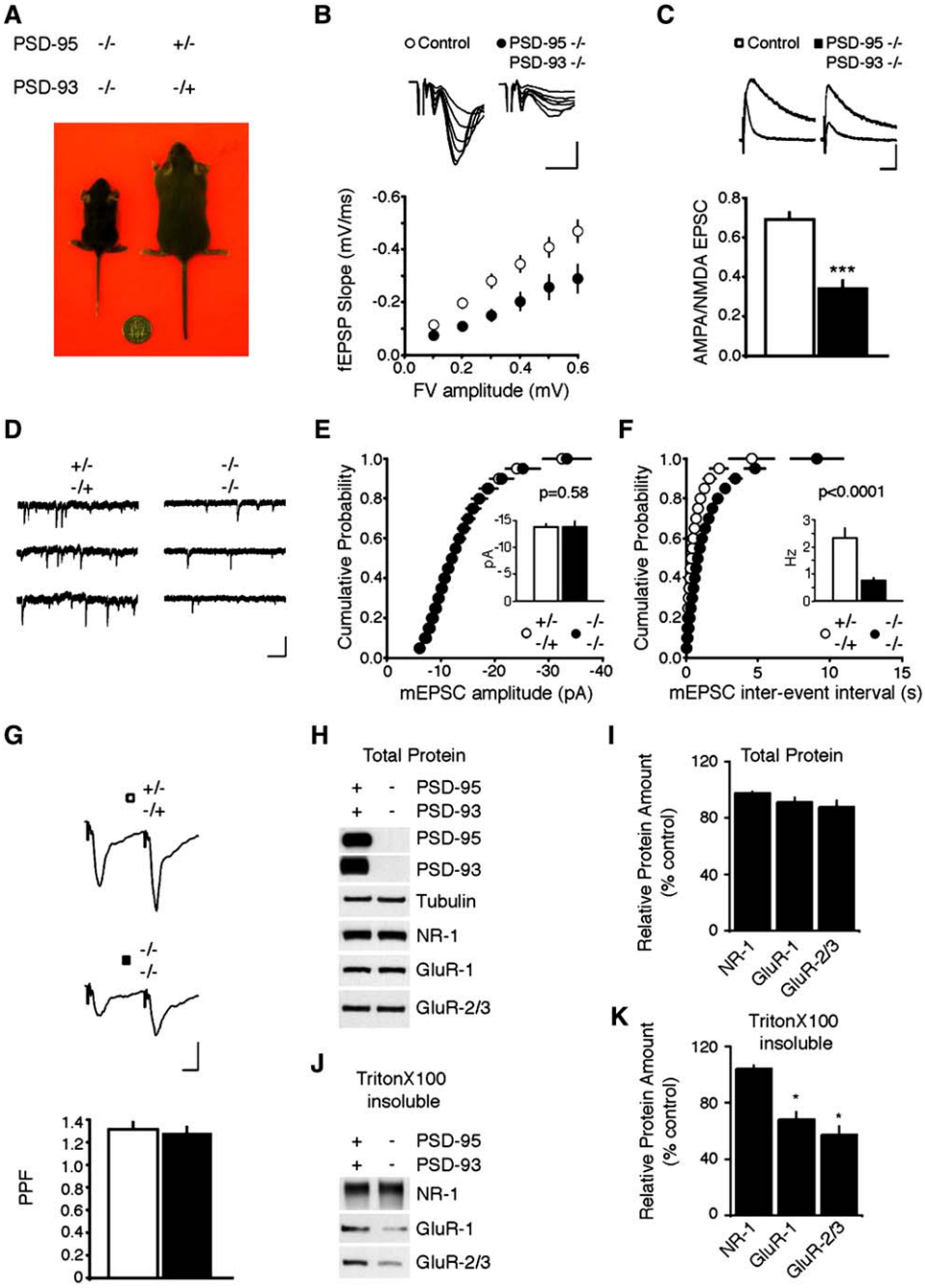

Figure 4. Impaired AMPA-R-Mediated Synaptic Transmission in PSD-95/PSD-93 Double KO Mice

(A) P32 PSD-95$^{-/-}$/PSD-93$^{-/-}$ and PSD-95$^{+/-}$ /PSD-93$^{-/+}$ littermates (U.S. dime shown for size reference).

(B) (Top) Traces of AMPA-R-mediated field responses recorded from PSD-95$^{-/-}$/PSD-93$^{-/-}$ and controls. Scale bar, 0.5 mV, 5ms. (Bottom) Input-output curve showing a reduction in the input-output relation in PSD-95$^{-/-}$/PSD-93$^{-/-}$ (controls: n = 56; PSD-95$^{-/-}$/PSD-93$^{-/-}$: n = 15; $p < 0.05$ for FV = 0.2–0.6).

(C) (Top) NMDA-R and AMPA-R EPSCs recorded in pyramidal neurons from PSD-95$^{-/-}$/PSD-93$^{-/-}$ and controls. Scale bar, 25 pA, 50 ms. (Bottom) AMPA/NMDA EPSC ratio bar graphs showing a reduction in PSD-95$^{-/-}$/PSD-93$^{-/-}$ mice (control: 0.69 ± 0.04, n = 40; PSD-95$^{-/-}$/PSD-93$^{-/-}$: 0.34 ± 0.04, n = 8; ***$p < 0.001$).

(D–F) mEPSC sample traces ([D], scale bar, 25 pA, 250 ms) and cumulative probability distributions showing no change in mEPSC amplitude (E) but a significant reduction in mEPSC frequency (F) in PSD-95$^{-/-}$/PSD-93$^{-/-}$ mice (control: n = 16; PSD-95$^{-/-}$/PSD-93$^{-/-}$: n = 13).

(G) PPF sample traces (top; scale bar: 0.25 mV, 10 ms) and summary (bottom) showing no difference between PSD-95$^{-/-}$/PSD-93$^{-/-}$ and controls (controls: 1.3 ± 0.06, n = 21; PSD-95$^{-/-}$/PSD-93$^{-/-}$: 1.28 ± 0.06, n = 17; $p = 0.97$).

(H and I) Total glutamate receptor levels in PSD-95$^{-/-}$/PSD-93$^{-/-}$ mice are unchanged. Western blotting of SDS-solubilized homogenates of PSD-95$^{-/-}$/PSD-93$^{-/-}$and littermate controls reveals no difference in total NR-1, GluR1, or GluR2/3 levels (n = 4).

(J and K) In TritonX 100 insoluble, PSD-enriched membrane fraction, GluR1 and GluR2/3 are reduced ~30%, whereas there is no change in NR-1 (n = 3, *$p < 0.05$).

Error bars = SEM.

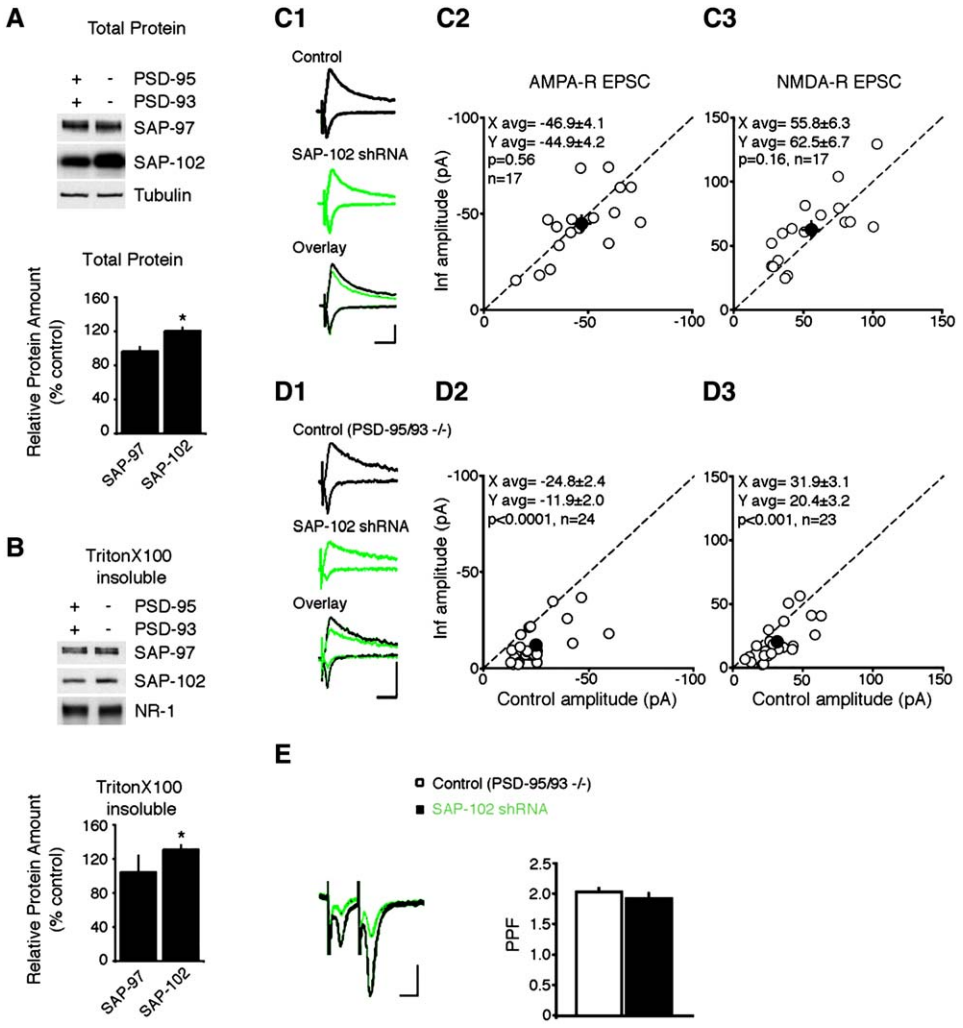

Figure 5. Functional Compensation by SAP-102 in PSD-95/PSD-93 Double KO Mice

(A) SAP-102 protein level increases in hippocampal homogenates of 4 week old PSD-95$^{-/-}$/PSD-93$^{-/-}$ (n = 4, *p < 0.05).

(B) Elevated amount of SAP-102, but not SAP-97, in TritonX 100 insoluble, PSD-enriched fraction from PSD-95$^{-/-}$/PSD-93$^{-/-}$ hippocampal membranes. NR-1 is shown as a loading control (n = 3, *p < 0.05).

(C1–D3) Open and filled circles represent amplitudes for single pairs and mean ± SEM, respectively. (C1) Traces of evoked EPSCs from an uninfected wild-type neuron (top) and a neighbor expressing SAP-102 shRNA (middle). Distributions of EPSCs show no effect of SAP-102 shRNA expression on AMPA-R EPSCs (C2) or NMDA-R EPSCs (C3). (D1) Traces of EPSCs in pyramidal neurons from PSD-95$^{-/-}$/PSD-93$^{-/-}$ mice showing that SAP-102 knockdown reduces the AMPA-R EPSC (D2) and modestly reduces the NMDA-R EPSC (D3). Scale bars for (C1) and (D1), 25 pA, 50 ms.

(E) PPF [sample traces, left (scale bars: 10 pA, 25 ms); and summary bar graphs, right] was not affected by SAP-102 shRNA expression in neurons from PSD-95$^{-/-}$/PSD-93$^{-/-}$ mice (uninfected: 2.0 ± 0.06, n = 21; infected: 1.9 ± 0.09, n = 21; p = 0.16).

Error bars = SEM.

reduction in the AMPA-R EPSC. These effects were specific, as a control shRNA construct had no effect, and expressing the PSD-95 or PSD-93 shRNAs in the PSD-95$^{-/-}$ or PSD-93$^{-/-}$ mice, respectively, were without effect. Interestingly, knockdown of PSD-95 or PSD-93 completely removed AMPA-Rs from largely nonoverlapping subpopulations of synapses without affecting the remaining synapses. This finding indicates heterogeneity among excitatory synapses. The nature of the heterogeneity is not obvious, because immunocytochemistry in dissociated neurons demonstrates that PSD-95 and PSD-93 puncta closely colocalize, and virtually all excitatory synapses in cells expressing shRNA for PSD-95 lack PSD-95 staining, but do stain for PSD-93 (Figure S1). However, electron microscopic immunogold studies have shown that colocalization of PSD-95 and PSD-93 is much lower in vivo (~30%) than that observed in vitro (>90%; Sans et al., 2000). Thus, it could be envisaged that AMPA-Rs are removed from synapses only when the level of PSD-MAGUKs falls below a critical threshold, and that in those synapses that remain unaltered in a single shRNA experiment, the unaffected PSD-MAGUK is above threshold levels. shRNA knockdown of SAP-102 had no significant effect on synaptic transmission at mature synapses, indicating that both PSD-95 and PSD-93, but not SAP-102, play an important role in maintaining AMPA-Rs at mature excitatory synapses.

Our findings show that shRNA-mediated knockdown of either PSD-95 or PSD-93 results in an ~50%

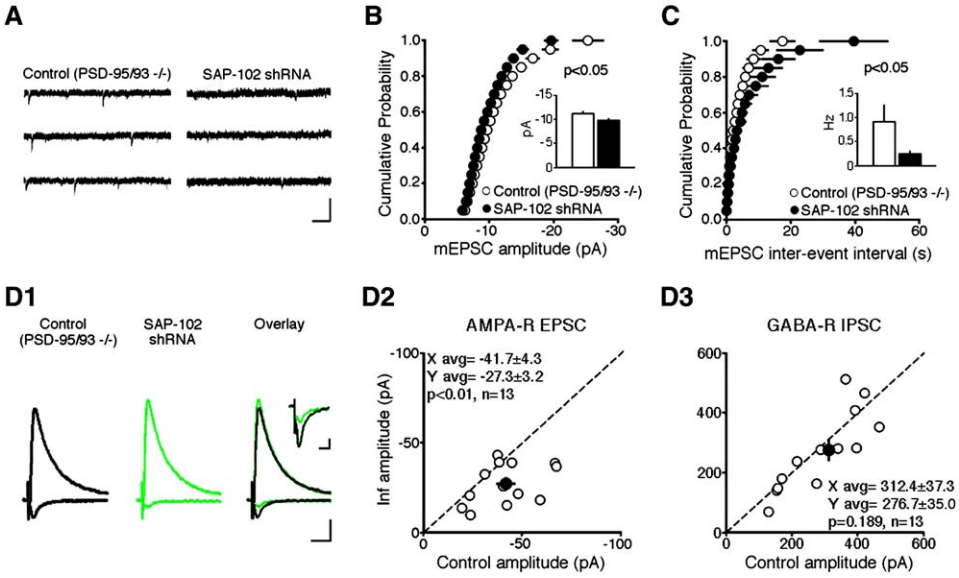

Figure 6. SAP-102 shRNA Expression in PSD-95/PSD-93 KO Mice Reduces mEPSC Amplitude and Frequency

(A–C) AMPA-R-mediated mEPSC traces ([A], scale bar, 25 pA, 250 ms) and cumulative distributions showing that shRNA-mediated knockdown of SAP-102 in PSD-95$^{-/-}$/PSD-93$^{-/-}$ mouse slice culture reduced the mEPSC amplitude ([B], n = 13) and frequency ([C], n = 13). Error bars = SEM. (D1–D3) shRNA of SAP-102 in pyramidal neurons from PSD-95$^{-/-}$/PSD-93$^{-/-}$ mice reduces AMPA-R EPSCs, but not IPSCs. (D1) Traces of evoked EPSCs (downward deflection) and IPSC (upward deflection) from an uninfected neuron (left) and a neighbor expressing SAP-102 shRNA (middle). Overlay inset shows the evoked EPSCs on a larger scale. (D2 and D3) Distributions of EPSCs showing that SAP-102 shRNA expression reduces AMPA-R EPSC (D2) but has no effect on $GABA_A$ IPSCs (D3). Open and filled circles represent amplitudes for single pairs and mean ± SEM, respectively. Scale bar, 50 pA, 50 ms. Inset scale bar, 10 pA, 25 ms.

reduction in AMPA-R EPSCs with a concomitant decrease in mEPSC frequency. Taken together with our findings in the PSD-95$^{-/-}$/PSD-93$^{-/-}$ mouse (see below), these results raised the possibility that PSD-95 and PSD-93 determine the synaptic targeting of most, if not all, AMPA-Rs at mature synapses. Indeed, simultaneous shRNA-mediated knockdown of PSD-95 and PSD-93 had additive effects, reducing AMPA-R transmission by substantially more than 50%.

Single shRNA for PSD-95 or PSD-93 selectively reduces AMPA-R transmission, whereas simultaneous double shRNA reduces both AMPA-R and NMDA-R EPSCs. A number of control experiments established that this reduction in the NMDA-R EPSC was specific. This suggests that PSD-95 and PSD-93 are key structural scaffolding elements of the PSD jointly required for proper synaptic expression of NMDA receptors.

The loss of synaptic AMPA-Rs induced by knockdown of PSD-95 was accompanied by an increase in the number of AMPA-Rs on extrasynaptic membranes, whereas the accumulation of synaptic AMPA-Rs with PSD-95 overexpression diminished extrasynaptic receptors (Schnell et al., 2002). This highlights the dynamic exchange of AMPA-Rs between the synaptic and extrasynaptic compartments.

Targeted Gene Knockout of PSD-95 and PSD-93

We have examined synaptic transmission in the hippocampus of mice lacking PSD-95 protein (Yao et al., 2004). As previously found in mice that express a truncated PSD-95 (Migaud et al., 1998), we found no defect in excitatory transmission in PSD-95$^{-/-}$ mice completely lacking PSD-95 protein. We have also studied synaptic transmission in the hippocampus in the PSD-93$^{-/-}$ mouse (McGee et al., 2001) and found that synaptic transmission is normal. Given the findings with shRNA, these negative results strongly imply that compensation occurs in the case of loss of a single PSD-MAGUK. Indeed, AMPA-R-mediated synaptic transmission in the PSD-95$^{-/-}$/PSD-93$^{-/-}$ mouse was reduced by 55%. As in the shRNA experiments, the defect in synaptic transmission was due to the all-or-none silencing of a population of synapses.

What might account for the remaining synaptic transmission in the absence of PSD-95 and PSD-93? Knockdown of SAP-102 in the PSD-95$^{-/-}$/PSD-93$^{-/-}$ mouse removed 53% of the remaining synaptic transmission. In this situation, the NMDA-R EPSC was also reduced, but not to the same extent as the AMPA-R EPSC. Considering that transmission is reduced by 55% in the double KO, the remaining transmission in cells expressing shRNA for SAP-102 is only ~15% of normal. These results suggest that nearly all synaptic AMPA-Rs require a PSD-MAGUK for proper synaptic targeting.

PSD-MAGUK-Dependent AMPA-R Synaptic Targeting Is Developmentally Regulated

The role of various PSD-MAGUKs in synapse development is controversial. In dissociated neuronal cultures PSD-95 is reported to be the first PSD-MAGUK scaffolding protein present at nascent postsynaptic sites (El-Husseini et al., 2000; Rao et al., 1998). However, other studies in intact brain suggest that PSD-95 is present at low levels in the early postnatal period, while SAP-102 is expressed at high levels (Sans et al., 2000). We have found that at early stages of synaptic

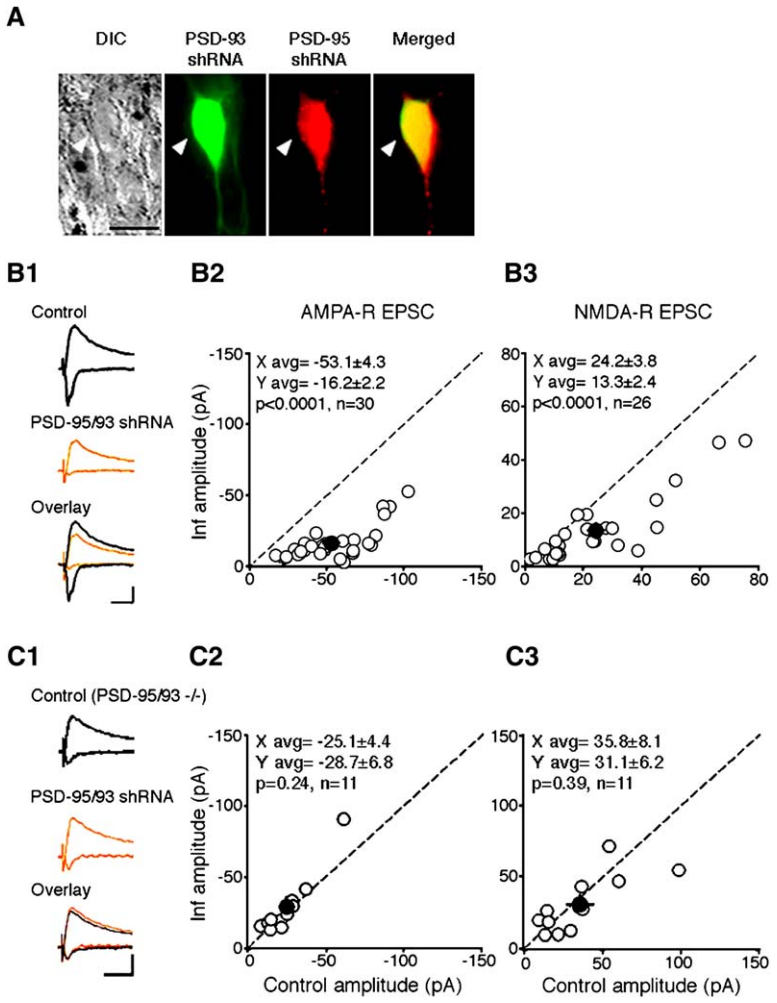

Figure 7. Dual shRNA-Mediated Knockdown of PSD-95 and PSD-93 in Single Neurons

(A) DIC image of a hippocampal pyramidal neuron (left, white arrow) doubly infected with Lentivirus encoding PSD-93 shRNA with EGFP and PSD-95 shRNA with dsRed. Merged EGFP and dsRed fluorescent images shown on the right. Scale bar, 50 μm. (B1 and C1) Traces of evoked EPSCs from an uninfected neuron (top) and a neighbor doubly expressing PSD-95 and PSD-93 shRNA (middle) in (B1) wild-type rat and (C1) PSD-95$^{-/-}$/PSD-93$^{-/-}$ mouse slice culture. Scale bar, 50 pA, 50 ms. For scatter plots open and filled circles represent amplitudes for single pairs and mean ± SEM, respectively. (B2–B3) EPSC amplitudes show a large reduction in the AMPA-R EPSC (B2) and a small reduction in the NMDA-R EPSC (B3) in wild-type slices. (C2–C3) Distribution of EPSCs showing no effect of simultaneous PSD-95 and PSD-93 shRNA expression on AMPA-R or NMDA-R EPSC amplitudes in PSD-95$^{-/-}$/PSD-93$^{-/-}$ mouse slices.

differentiation, transmission does not require either PSD-95 or PSD-93. Rather, SAP-102 mediates synaptic AMPA-R clustering in neonates. This is consistent with the developmental expression of PSD-MAGUKs in the hippocampus. We know that the effect of acute knockdown of SAP-102 on AMPA-R-mediated transmission is specific because NMDA receptor transmission is not affected. This suggests that SAP-102 is necessary for AMPA-R trafficking to synapses that have already been formed and contain only NMDA receptors. The functional relevance of the developmental switch in PSD-MAGUK-dependent AMPA-R trafficking remains unclear. PSD-MAGUKs differ in their ability to interact with synaptic proteins. Presumably these differential binding abilities confer specific functions, independent of AMPA-R trafficking.

How Do PSD-MAGUKs Traffic AMPA-Rs?

Since most PSD-MAGUKs do not bind directly to AMPA-Rs, an intermediary protein must be involved. We previously showed that the transmembrane protein stargazin and other members of the TARP family likely serve this role (Chen et al., 2000; Schnell et al., 2002; Tomita et al., 2003). TARPs bind directly to AMPA-Rs and to the first two PDZ domains of PSD-MAGUKs. It will be interesting to determine how general the PSD-MAGUK-TARP trafficking mechanism is at other synapses in the central nervous system. What holds PSD-MAGUKs at the PSD? There are a number of candidates, but recent attention has focused on neuroligins, which are transmembrane cell adhesion proteins, that bind PSD-MAGUKs and are implicated in early steps of synapse formation (Chih et al., 2005; Graf et al., 2004; Irie et al., 1997; Nam and Chen, 2005). However, the fact that neuroligins bind to the third PDZ domain, whereas targeting of PSD-95 relies only on the first two PDZ domains (Craven et al., 1999), casts doubt on their role in AMPA-R clustering.

A number of issues remain to be addressed. We have found that, except for SAP-97, the other PSD-MAGUKs appear to function in a similar manner. What advantage is conferred by this redundancy? One obvious advantage is robustness; if one member of the family is lost, the synapses can still function. Might different PSD-MAGUKs have distinct effects on other processes involved in synaptic function? Most evidence in this and previous studies emphasizes a role of PSD-MAGUKs in the constitutive trafficking of AMPA-Rs. Might the PSD-MAGUK-dependent trafficking be activity dependent? Previous results examining the effects of palmitoylation of PSD-95 suggest that this may be the case

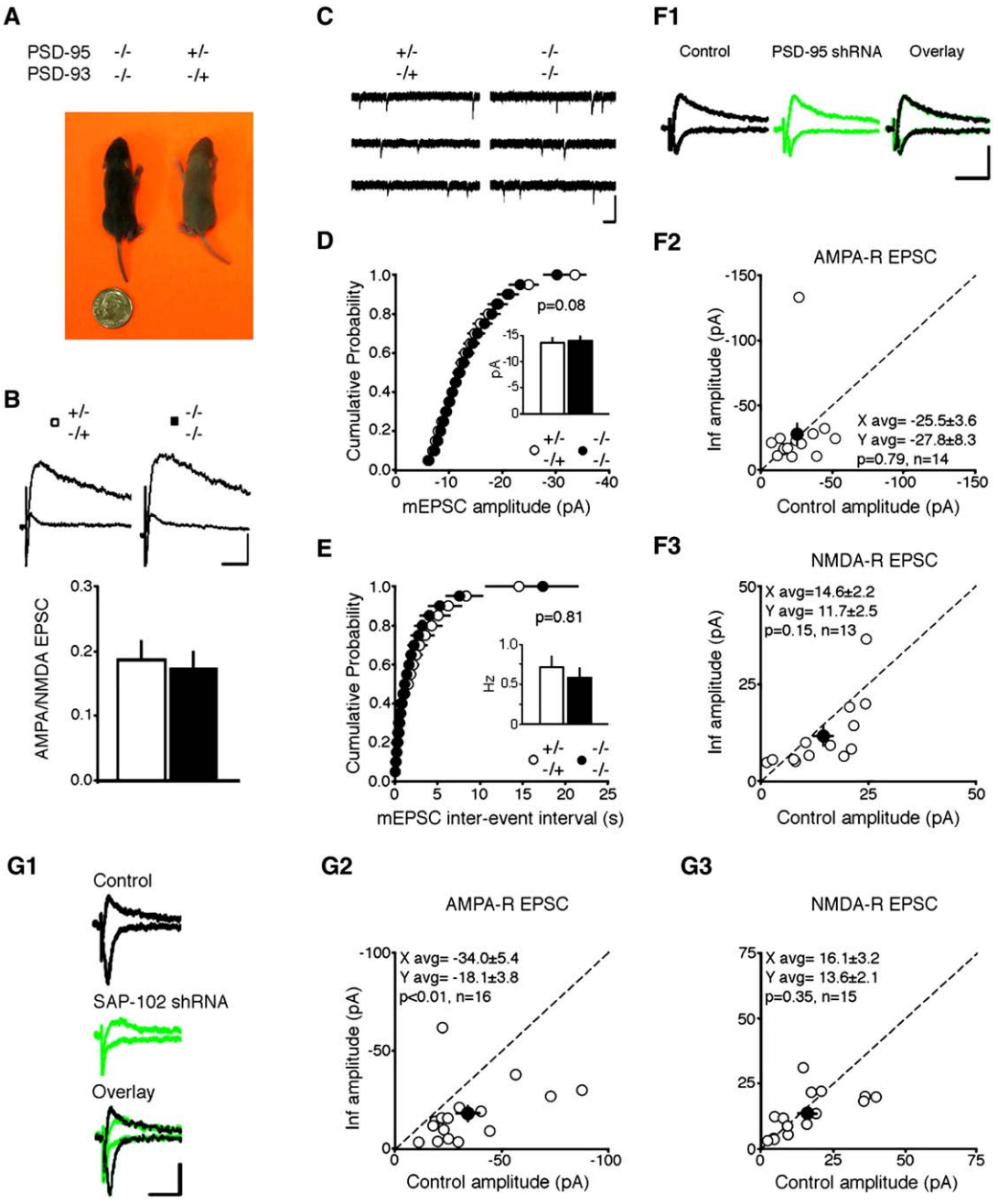

Figure 8. PSD-MAGUK AMPA-R Trafficking in Neonatal Mice

(A) P8 PSD-95$^{-/-}$/PSD-93$^{-/-}$ and PSD-95$^{+/-}$/PSD-93$^{-/+}$ littermates are not obviously different in size (U.S. dime shown for size reference).

(B) (Top) NMDA-R and AMPA-R EPSCs from representative cells from PSD-95$^{-/-}$/PSD-93$^{-/-}$ and controls. Scale bar, 25 pA, 50 ms. (Bottom) Summary bar graphs showing no significant difference in the AMPA/NMDA EPSC ratio (controls: 0.19 ± 0.03, n = 21; PSD-95$^{-/-}$/PSD-93$^{-/-}$: 0.17 ± 0.02, n = 13; p = 0.75).

(C–E) mEPSC sample traces ([C], scale bar: 25 pA, 250 ms) and probability distributions showing no change in mEPSC amplitude (D) or mEPSC frequency (E) (controls: n = 17; PSD-95$^{-/-}$/PSD-93$^{-/-}$: n = 12).

(F1–G3) Open and filled circles represent amplitudes for single pairs and mean ± SEM, respectively. (F1) Traces of evoked EPSCs from an uninfected neuron (left) and a neighbor expressing PSD-95 shRNA (middle) in wild-type immature slice cultures. Scale bar, 25 pA, 50 ms. Distributions of EPSC amplitudes show no significant difference in the AMPA-R EPSC (F2) or NMDA-R EPSC (F3). (G1) Traces of evoked EPSCs from an uninfected P8 neuron (top) and a neighbor infected with SAP-102 shRNA (middle) in wild-type immature slice cultures. Scale bar, 20 pA, 50 ms. Distributions of EPSC amplitudes show a significant reduction in the AMPA-R EPSC in cells expressing SAP-102 shRNA (G2) with no change in the NMDA-R EPSC (G3).

(El-Husseini Ael et al., 2002) and that the enhancement in synaptic transmission caused by overexpression of PSD-95 occludes long-term potentiation (LTP) and enhances long-term depression (LTD) (Ehrlich and Malinow, 2004; Stein et al., 2003). It will be interesting to determine whether endogenous PSD-MAGUKs have a role

in regulating AMPA-R synaptic expression during bidirectional synaptic plasticity. If so, it will be of interest to determine how CaMKII, a key kinase involved in LTP, regulates PSD-MAGUK-dependent AMPA-R trafficking.

Experimental Procedures

Plasmid Constructs

shRNA oligonucleotides were inserted into pLLox3.7. The following shRNA targeting sequences were used for PSD-95 TCACG ATCATCGCTCAGTATA; PSD-93 GACTGCCTAGCCAAGGACTTA (alternative sequence: CTCTATTGTTCGACTGTATAT; both sequences yielded similar results); SAP-102 CCAAGTCCATCGAAGC ACTTA. For knockdown of SAP-102 in mouse, the following targeting sequence was used with comparable efficiency (data not shown), with the single nucleotide difference indicated: CCAAGTC CATTGAAGCACTTA. Targeting sequences for PSD-95 and PSD-93 completely overlap in mouse and rat; rat cDNAs of PSD-95, PSD-93, SAP-97, and SAP-102 were inserted into pGWI vector. Silent mutations in cDNA pointmutant constructs were generated using QuickChangeII (Stratagene) following the manufacturer's instructions.

Antibodies

Mouse PSD-95 antibody was from ABR. Rabbit anti-GluR2/3 and anti-GluR1 and mouse anti-GluR2 were obtained from Chemicon. Mouse NR-1 antibody was from Pharmigen. Mouse Tubulin and goat actin antibodies were from Santa Cruz. PSD-93 antibody was from Zymed. Guinea pig SAP-102 was described in Firestein et al. (1999). Rabbit SAP-97 antibody was described in Topinka and Bredt (1998).

Overexpression

COS-7 cells were transfected with Lipofectamine 2000 with cDNA expression vectors as well as corresponding shRNA vectors in a molar ratio of 1:3. Forty-eight hours after transfection cells were lysed with SDS-PAGE sample buffer. Lysates were sonicated and denatured at 67°C for 10 min and analyzed by SDS-PAGE. Blots were probed with antibodies PSD-95 (1:1000), PSD-93 (1:2000), SAP-97 (1:2000) and SAP-102 (1:2000). Actin served as a loading control for each blot. Immunoreactivity was visualized with the ECL system (Pierce).

Neuronal Culture and Transfection

Dissociated hippocampal neuron cultures were prepared as previously described (Craven et al., 1999). In short, embryonic day 18 (E18) rat pups were sacrificed, and hippocampi were isolated and digested using papain protease. Neurons were dissociated and resuspended in Neurobasal medium containing B27, Glutamax, and antibiotics (all Invitrogen). Neurons were plated at 50K or 100K per cm^2 on Poly-D-lysine-treated support. Hippocampal neurons were transfected at DIV 14–16 with 0.5–1 μg pLLox3.7 vectors using 0.5–1 μl Lipofectamine 2000 (Invitrogen) and incubated for 5 more days before analysis.

Immunocytochemistry and Surface GluR2 Staining

Transfected neurons were used for immunocytochemistry at DIV 14–16+5. Neurons were fixed with 4% paraformaldehyde/4% sucrose in PBS for 12 min on ice followed by 100% methanol for 10 min at –20°C, washed twice with PBS for 5 min on ice. Cells were permeabilized with 0.1% TritonX 100 in PBS for 10 min and washed with PBS for 5 min. After blocking with normal goat serum (3%) in PBS for 1 hr, the cells were incubated with mouse anti-PSD-95 (1:1000) and rabbit anti-PSD-93 (1:1000) antibodies followed by Alexa 546 or 647 conjugated secondary antibodies (Molecular Probes). Images were captured with a laser scanning fluorescent microscope LSM510 (Carl Zeiss) equipped with a 63× oil emersion objective. Colocalization was analyzed using LSM510 analysis software. At least 500 PSD-93 positive clusters were analyzed for PSD-95 colocalization in at least seven independent cells per condition. Statistical significance was determined by Student's t test.

Surface GluR2 staining was performed as described in Wyszynski et al. (2002). In short, surface GluR2 receptors were "live"-labeled with an antibody to an extracellular epitope of GluR2 (Chemicon) by incubating neurons in conditioned medium for 15 min at 37°C. Neurons were fixed with 4% paraformaldehyde/4% sucrose/PBS for 8 min and blocked with PBS containing 3% normal goat serum. Surface GluR2 was visualized with Alexa 546 conjugated secondary antibody. Stacks of fluorescent images were acquired with a LSM Pascal confocal laser microscopy system (Carl Zeiss) with a 63× oil emersion objective. Quantification was carried out on proximal dendrites in at least nine independent, transfected neurons. For quantification of spine localization of surface GluR2 clusters, only mushroom-shaped protrusions from the dendrite as visualized by GFP expression were analyzed using LSM Pascal colocalization analysis software. A spine was considered GluR2 positive if it colocalized with at least one surface GluR2 cluster. The total number of spines along the analyzed dendrite was recorded. The length of a given dendrite was measured using LSM Pascal analysis software tools (Carl Zeiss). The number of spines was then normalized to 10 μm. Filopodia-like protrusions were excluded from the analysis. At least 250 spines were analyzed under each condition. Total surface GluR2 staining was assessed with the following criteria. Surface GluR2 clusters colocalized with the GFP marker anywhere on the dendrite were analyzed. The number of clusters along the dendrite was counted and the length of the analyzed dendrite was measured using LSM Pascal analysis software tools. The number of clusters was normalized to 10 μm. At least 275 surface GluR2 clusters were analyzed in each condition in at least nine independent neurons. Statistical significance was determined by Student's t test.

Lentivirus Production and Neuronal Infection

For Lentiviral particle production, HEK293T cells were cotransfected with pLLox3.7 and helper vectors pDelta8.9 and pVSVg using Lipofectamine 2000 (Invitrogen). Forty-eight hours after transfection, supernatant was collected and concentrated by ultrafiltration in Centricon Plus 100 (Millipore). Particles were aliquoted and stored at −80°C. Particle titer was determined by infection of HEK293T cells. Forty-eight hours after infection, HEK293T cells were analyzed with a FACScalibur flow cytometer to determine titer.

Dissociated hippocampal neurons (see above) were infected at DIV 9–10 with MOI 2 and incubated for 6 more days in the presence of 5-Fluorodeoxyuridine and Uridine (Sigma). This achieved about 70% of infection efficiency. Neurons were then lysed with SDS-PAGE sample buffer. Lysates were analyzed with SDS-PAGE and western blotting. Blots were probed with PSD-95, PSD-93, SAP-97, and SAP-102 as described above as well as anti NR-1 (1:2000) and anti Tubulin (1:1000) as loading controls.

Brain Lysates and Solubilization

PSD-95/PSD-93 double knockout mice and littermate control animals were sacrificed and the hippocampus was isolated. Hippocampi were homogenized in 10 volumes H-Buffer (320 mM sucrose, 2 mM EDTA, 20 mM TrisHCl [pH 8.0], 1 mM PMSF). Homogenate was centrifuged for 10 min at 1000 × g. Supernatants S1 were used for further experiments. For total protein extracts SDS was added to a final concentration of 1% and agitated for 1 hr at 4°C. Extracts were sonicated and the protein concentration was determined by Bradford assay. Twenty-five micrograms of total protein was loaded per lane and analyzed by SDS-PAGE and western blotting. P2 crude synaptosome fractions, prepared from the supernatant S1, were resuspended in an equal volume of TET buffer (1% TritonX 100, 2 mM EDTA, 20 mM TrisHCl [ph 7.4], 1 mM PMSF) and agitated for 1 hr at 4°C. Extracts were centrifuged at 100,000 × g for 1 hr. The supernatant is the TritonX 100 soluble fraction. The pellet was resuspended in 0.1 vol of 1% SDS, 2 mM EDTA, and 20 mM TrisHCl (pH 7.4). Then 0.9 volume of TET buffer was added and the extracts agitated for 1 hr at 4°C (Tomita et al., 2005). Protein concentration was determined by Bradford assay. Five micrograms of protein were loaded per lane and analyzed by SDS-PAGE followed by western blotting. Desitometric analysis was carried out using ImageJ software. Significance was determined by Student's t test.

Electrophysiology in Acute Slices

Transverse hippocampal slices (300–400 μm thick) were prepared from PSD-$95^{-/-}$, PSD-$93^{-/-}$, PSD-$95^{-/-}$/PSD-$93^{-/-}$, heterozygous, and wild-type littermates (7–40 days old) as previously described

(Luscher et al., 2000). To preclude bias, the experimenter was blind to the genotype of the mice during fEPSP and AMPA/NMDA ratio experiments (except while using PSD-95$^{-/-}$/PSD-93$^{-/-}$mice, which were always clearly smaller than their littermate controls). Acute recordings were done at room temperature (24°C–28°C). Perfusion medium contained (in mM) 119 NaCl, 2.5 KCl, 1.3 $MgSO_4$ (4 $MgSO_4$, to measure AMPA/NMDA ratios and mEPSCs), 1 NaH_2PO_4, 26.2 $NaHCO_3$, 11 glucose, 2.5 $CaCl_2$ (4 $CaCl_2$, for AMPA/NMDA ratios and mEPSCs), and 0.1–0.15 picrotoxin, saturated with 95% O_2/5% CO_2. Inputs from CA3 to CA1 were severed to prevent propagation of epileptic form activity.

Field EPSP recordings were made in CA1 stratum radiatum following stimulation of Schaffer collaterals with monopolar glass electrodes filled with 1 M NaCl. Synaptic responses were recorded with glass electrodes (3–5 MΩ) filled with 1 M NaCl using a MultiClamp 700A amplifier (Axon Instruments). PPF was obtained by delivering two stimuli at an interval of 40 ms. For experiments involving P30–40 animals, slices from each knockout genotype and control were interleaved in a given day. Thus, we generated complete input-output curves for each knockout genotype with respective control littermates. Statistical analyses showed no significant difference between control groups. Thus, we combined the controls and compared knockout values to this pooled control value.

Somatic whole-cell voltage-clamp recordings were made from visually identified CA1 pyramidal neurons using 3–5 MΩ glass electrodes filled with internal recording solution containing (in mM) 125 $CsMeSO_3$, 2.5 CsCl, 7.7 TEA, 5 QX-314, 4 Mg-ATP, 0.3 Na-GTP, 20 HEPES, 8 NaCl, and 0.2 EGTA (or 10 BAPTA) (pH 7.2) at 280–290 mOsm. Series and input resistance were monitored, and cells in which either parameter varied by 25% during a recording session were discarded. AMPA-R and NMDA-R EPSCs were obtained by evoking dual component responses while voltage-clamping neurons at +40 mV. One hundred micromolar APV (or ten micromolar CPP) was then added to obtain the pure AMPA-R EPSC, and the NMDA-R component was derived by subtracting the AMPA-R EPSC from the compound EPSC. Interstimulus interval was 10 s. For experiments using BAPTA, responses were evoked 2 min after establishing whole-cell configuration. For recordings not using BAPTA, only cells in which the AMPA-R EPSC after NMDA-R blockade did not differ from baseline responses recorded at −70 mV before voltage-clamping at +40 mV were included in the final analysis. For experiments involving P30–40 animals, we generated complete AMPA/NMDA EPSC ratios for each knockout genotype with respective control littermates. Statistical analyses showed no significant difference between control groups. Thus, we combined the controls and compared knockout values to this pooled control value. mEPSCs were recorded at −70 mV in the presence of 0.5 μM tetrodotoxin, 0.1–0.15 mM picrotoxin, and 50 mM sucrose to increase the frequency of events. mEPSCs were analyzed off line with customized software using a threshold of 4 pA. All data are expressed as mean ± SEM. Statistical significance was determine using two-tail unpaired t tests for between-group comparisons. For mEPSCs, the statistical significance between distributions was determined using Kolmogorov-Smirnov test.

Electrophysiology in Slice Culture

Standard procedures were used to prepare rat and mouse organotypic slice cultures from animals ranging from P2–9 (Schnell et al., 2002; Stein et al., 2003). All RNAi slice culture experiments (except those described in Figures 8F1–8G3) were carried out in *mature slices* (see Figure 9). Experiments described in Figures 8F1–8G3 were carried out using *immature slices* (see Figure 9). All slice cultures were injected near the pyramidal cell layer with shRNA-containing Lentiviral particles at a titer ranging from 10^6–10^8 cfu/ml.

Synaptic responses were evoked from pairs of infected and uninfected neurons simultaneously by electrically stimulating a common pathway with monopolar glass electrodes filled with external perfusion medium (see below). Recordings were made from pairs of pyramidal neurons using 3–5 MΩ glass electrodes filled with an internal solution containing (in mM) 115 $CsMeSo_3$, 20 CsCl, 10 HEPES, 2.5 $MgCl_2$, 4 Mg-ATP, 0.4 Na-GTP, 0.6 EGTA, and 5 QX-314 (pH 7.2) at 290–300 mOsm. For experiments described in Figures 6D1–6D3 the following intracellular recording solution was used (in mM): 107.5 Cs-gluconate, 20 HEPES, 0.2 EGTA, 8 Na-gluconate, 8 TEA-Cl, 4 Mg-ATP, 0.3 Na_3-GTP, and 5 QX-314 (pH 7.2) at 290 mOsm. External perfusion medium consisted of (in mM) 119 NaCl, 2.5 KCl, 4 $MgSO_4$, 1 NaH_2PO_4, 26.2 $NaHCO_3$, 11 glucose, and 4 $CaCl_2$, saturated with 95% O_2/5% CO_2 and including 100–150 μM picrotoxin and 5–10 μM 2-Chloroadenosine to block inhibition and suppress epileptic activity. Series and input resistance were monitored and cells were discarded if they differed by more than 20%. AMPA-R EPSCs were evoked while voltage clamping cells at −70 mV, and the amplitude was determined by measuring the peak of this response. NMDA-R EPSCs were obtained while voltage clamping cells at +40 mV, and the magnitude was determined by measuring the amplitude of the EPSCs 60−100 ms after the shock artifact. Statistical difference was determined using a two-tailed paired t test.

mEPSCs were recorded at −70 mV in the presence of 0.5 μM tetrodotoxin, 0.1–0.15 mM picrotoxin, and 50 mM sucrose to increase the frequency of events (100 mM sucrose was added for experiments described in Figures 6A–6C). mEPSCs were analyzed off line with customized software using a threshold of 4 pA. For mEPSCs, statistical significance between distributions was determined using a Kolmogorov-Smirnov test. Somatic outside-out patches were clamped at −70 mV. AMPA-R currents were evoked by local application of 500 mM S-AMPA for 2 s in the presence of 100 μM cyclothiazide. Minimal stimulation experiments were carried out as previously described (Stein et al., 2003).

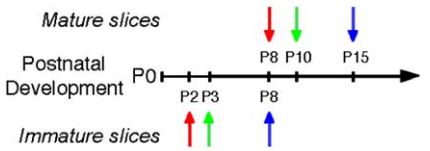

Figure 9. Slice Culture Scheme

Mature slices were made by plating the hippocampus of P8 (P8 arrow, top) animals, followed by Lentiviral infection 2 days later (P10 arrow), and assaying synaptic transmission starting 5 days after infection (P15 arrow). Immature slices were made by plating the hippocampus of P2 animals (P2 arrow, bottom), infecting 1 day later (P3 arrow), and assaying synaptic transmission starting 5 days after infection (P8 arrow, bottom).

Supplemental Data

The Supplemental Data for this article can be found online at http://www.neuron.org/cgi/content/full/52/2/307/DC1/.

Acknowledgments

We would like to thank Carlos Lois (Massachusetts Institute of Technology) for providing the pLLX3.7 shRNA and helper vectors, Keith Brown for technical assistance with the mouse colony, and members of the Nicoll lab and Bredt lab and Laura A.B. Elias for invaluable input throughout the project. G.M.E. is supported by Genentech Inc. and Sandler Family Graduate Research Fellowships. D.S.B. and R.A.N. are supported by funds from the NIH.

Received: May 15, 2006
Revised: August 7, 2006
Accepted: September 5, 2006
Published: October 18, 2006

References

Beique, J.C., and Andrade, R. (2003). PSD-95 regulates synaptic transmission and plasticity in rat cerebral cortex. J. Physiol. *546*, 859–867.

Chen, L., Chetkovich, D.M., Petralia, R.S., Sweeney, N.T., Kawasaki, Y., Wenthold, R.J., Bredt, D.S., and Nicoll, R.A. (2000). Stargazin regulates synaptic targeting of AMPA receptors by two distinct mechanisms. Nature *408*, 936–943.

Chih, B., Engelman, H., and Scheiffele, P. (2005). Control of excitatory and inhibitory synapse formation by neuroligins. Science *307*, 1324–1328.

Cho, K.O., Hunt, C.A., and Kennedy, M.B. (1992). The rat brain postsynaptic density fraction contains a homolog of the Drosophila discs-large tumor suppressor protein. Neuron *9*, 929–942.

Craven, S.E., El-Husseini, A.E., and Bredt, D.S. (1999). Synaptic targeting of the postsynaptic density protein PSD-95 mediated by lipid and protein motifs. Neuron *22*, 497–509.

Ehrlich, I., and Malinow, R. (2004). Postsynaptic density 95 controls AMPA receptor incorporation during long-term potentiation and experience-driven synaptic plasticity. J. Neurosci. *24*, 916–927.

El-Husseini, A.E., Schnell, E., Chetkovich, D.M., Nicoll, R.A., and Bredt, D.S. (2000). PSD-95 involvement in maturation of excitatory synapses. Science *290*, 1364–1368.

El-Husseini Ael, D., Schnell, E., Dakoji, S., Sweeney, N., Zhou, Q., Prange, O., Gauthier-Campbell, C., Aguilera-Moreno, A., Nicoll, R.A., and Bredt, D.S. (2002). Synaptic strength regulated by palmitate cycling on PSD-95. Cell *108*, 849–863.

Firestein, B.L., Firestein, B.L., Brenman, J.E., Aoki, C., Sanchez-Perez, A.M., El-Husseini, A.E., and Bredt, D.S. (1999). Cypin: a cytosolic regulator of PSD-95 postsynaptic targeting. Neuron *24*, 659–672.

Graf, E.R., Zhang, X., Jin, S.X., Linhoff, M.W., and Craig, A.M. (2004). Neurexins induce differentiation of GABA and glutamate postsynaptic specializations via neuroligins. Cell *119*, 1013–1026.

Irie, M., Hata, Y., Takeuchi, M., Ichtchenko, K., Toyoda, A., Hirao, K., Takai, Y., Rosahl, T.W., and Sudhof, T.C. (1997). Binding of neuroligins to PSD-95. Science *277*, 1511–1515.

Kim, E., Niethammer, M., Rothschild, A., Jan, Y.N., and Sheng, M. (1995). Clustering of Shaker-type K+ channels by interaction with a family of membrane-associated guanylate kinases. Nature *378*, 85–88.

Kistner, U., Wenzel, B.M., Veh, R.W., Cases-Langhoff, C., Garner, A.M., Appeltauer, U., Voss, B., Gundelfinger, E.D., and Garner, C.C. (1993). SAP90, a rat presynaptic protein related to the product of the Drosophila tumor suppressor gene dlg-A. J. Biol. Chem. *268*, 4580–4583.

Kornau, H.C., Schenker, L.T., Kennedy, M.B., and Seeburg, P.H. (1995). Domain interaction between NMDA receptor subunits and the postsynaptic density protein PSD-95. Science *269*, 1737–1740.

Lois, C., Hong, E.J., Pease, S., Brown, E.J., and Baltimore, D. (2002). Germline transmission and tissue-specific expression of transgenes delivered by lentiviral vectors. Science *295*, 868–872.

Luscher, C., Nicoll, R.A., Malenka, R.C., and Muller, D. (2000). Synaptic plasticity and dynamic modulation of the postsynaptic membrane. Nat. Neurosci. *3*, 545–550.

McGee, A.W., Topinka, J.R., Hashimoto, K., Petralia, R.S., Kakizawa, S., Kauer, F.W., Aguilera-Moreno, A., Wenthold, R.J., Kano, M., and Bredt, D.S. (2001). PSD-93 knock-out mice reveal that neuronal MAGUKs are not required for development or function of parallel fiber synapses in cerebellum. J. Neurosci. *21*, 3085–3091.

Migaud, M., Charlesworth, P., Dempster, M., Webster, L.C., Watabe, A.M., Makhinson, M., He, Y., Ramsay, M.F., Morris, R.G., Morrison, J.H., et al. (1998). Enhanced long-term potentiation and impaired learning in mice with mutant postsynaptic density-95 protein. Nature *396*, 433–439.

Nakagawa, T., Futai, K., Lashuel, H.A., Lo, I., Okamoto, K., Walz, T., Hayashi, Y., and Sheng, M. (2004). Quaternary structure, protein dynamics, and synaptic function of SAP97 controlled by L27 domain interactions. Neuron *44*, 453–467.

Nam, C.I., and Chen, L. (2005). Postsynaptic assembly induced by neurexin-neuroligin interaction and neurotransmitter. Proc. Natl. Acad. Sci. USA *102*, 6137–6142.

Rao, A., Kim, E., Sheng, M., and Craig, A.M. (1998). Heterogeneity in the molecular composition of excitatory postsynaptic sites during development of hippocampal neurons in culture. J. Neurosci. *18*, 1217–1229.

Rumbaugh, G., Sia, G.M., Garner, C.C., and Huganir, R.L. (2003). Synapse-associated protein-97 isoform-specific regulation of surface AMPA receptors and synaptic function in cultured neurons. J. Neurosci. *23*, 4567–4576.

Sans, N., Petralia, R.S., Wang, Y.X., Blahos, J., II, Hell, J.W., and Wenthold, R.J. (2000). A developmental change in NMDA receptor-associated proteins at hippocampal synapses. J. Neurosci. *20*, 1260–1271.

Schnell, E., Sizemore, M., Karimzadegan, S., Chen, L., Bredt, D.S., and Nicoll, R.A. (2002). Direct interactions between PSD-95 and stargazin control synaptic AMPA receptor number. Proc. Natl. Acad. Sci. USA *99*, 13902–13907.

Sheng, M. (2001). Molecular organization of the postsynaptic specialization. Proc. Natl. Acad. Sci. USA *98*, 7058–7061.

Stein, V., House, D.R., Bredt, D.S., and Nicoll, R.A. (2003). Postsynaptic density-95 mimics and occludes hippocampal long-term potentiation and enhances long-term depression. J. Neurosci. *23*, 5503–5506.

Tomita, S., Chen, L., Kawasaki, Y., Petralia, R.S., Wenthold, R.J., Nicoll, R.A., and Bredt, D.S. (2003). Functional studies and distribution define a family of transmembrane AMPA receptor regulatory proteins. J. Cell Biol. *161*, 805–816.

Tomita, S., Stein, V., Stocker, T.J., Nicoll, R.A., and Bredt, D.S. (2005). Bidirectional synaptic plasticity regulated by phosphorylation of stargazin-like TARPs. Neuron *45*, 269–277.

Topinka, J.R., and Bredt, D.S. (1998). N-terminal palmitoylation of PSD-95 regulates association with cell membranes and interaction with K+ channel Kv1.4. Neuron *20*, 125–134.

Wyszynski, M., Kim, E., Dunah, A.W., Passafaro, M., Valtschanoff, J.G., Serra-Pages, C., Streuli, M., Weinberg, R.J., and Sheng, M. (2002). Interaction between GRIP and liprin-alpha/SYD2 is required for AMPA receptor targeting. Neuron *34*, 39–52.

Yao, W.D., Gainetdinov, R.R., Arbuckle, M.I., Sotnikova, T.D., Cyr, M., Beaulieu, J.M., Torres, G.E., Grant, S.G., and Caron, M.G. (2004). Identification of PSD-95 as a regulator of dopamine-mediated synaptic and behavioral plasticity. Neuron *41*, 625–638.